Open access • Journal Article • DOI:10.1109/JSTQE.2019.2933788

Slow Light in Subwavelength Grating Waveguides — Source link

Philippe Jean, Antoine Gervais, Sophie LaRochelle, Wei Shi

Institutions: Laval University

Published on: 01 Mar 2020 - IEEE Journal of Selected Topics in Quantum Electronics (IEEE)

Topics: Slow light, Grating, Group velocity, Waveguide (optics) and Wavelength

Slow Light in Subwavelength Grating Waveguides

Philippe Jean, Antoine Gervais, Sophie LaRochelle and Wei Shi

Journal of Selected Topics in Quantum Electronics, (Early Access) (2019)

Doi: 10.1109/JSTQE.2019.2933788

https://ieeexplore.ieee.org/document/8790785

Slow Light in Subwavelength Grating Waveguides

Philippe Jean, Antoine Gervais, Sophie LaRochelle, *Senior Member, IEEE,* and Wei Shi, *Member, IEEE*

***Abstract*—Structural slow light is the dispersion engineering process by which the group velocity of light can be drastically reduced in a periodic waveguide structure. Enabling large group delay and enhancing the light-matter interaction on a subwavelength scale, on-chip slow light is of great interest in a vast array of fields such as non-linear optic, sensing, laser physics, telecommunication and computing. In this work, we experimentally demonstrate, for the first time, slow light in subwavelength grating waveguides on the silicon-on-insulator platform. We present a comprehensive numerical study in analytical modelling and 3D FDTD. Multiple waveguides variations were fabricated using an electron-beam lithography process. Figures of merit such as group index, bandwidth and loss-per-delay are examined in both theory and experiment. A maximum measured group index of 47.74 with a loss-per-delay of 103.37 dB/ns has been achieved near the wavelength of 1550 nm. A broad bandwidth of 8.82 nm was measured, in which the group index remains larger than 10. We also show that the region of slow light operation can be shifted over a large wavelength span by controlling a single design parameter.**

I. Introduction

SUBWAVELENGTH grating waveguides (SWG) on the silicon-on-insulator (SOI) platform have attracted significant research interest in the recent years due to their flexibility in engineering the refractive index of integrated waveguides [1], their use in high-efficiency fibre-to-chip couplers [2] and their potential in increasing the sensitivity of sensors [3], among others. SWGs are made of a periodic arrangement of silicon blocks of length L spaced by a distance Λ such that they support the propagation of a diffraction-less Bloch mode [4]. A standard silicon SWG waveguide of width W is schematically depicted in figure 1. The dispersion properties and Bloch mode profile of the SWG waveguide can be controlled by engineering the period-to-wavelength ratio and the ratio of silicon-to-cladding material along the propagation axis, or duty-cycle $DC = L/\Lambda$. SWGs can then behave as homogeneous metamaterials in the long-wavelength regime ($\lambda \gg \Lambda$), as Bragg mirrors in the band gap regime where mode propagation is forbidden ($\lambda \approx \Lambda$) or as slow light waveguides near the band-edge at the band gap lower-frequency limit. These peculiarities of the dispersion relation of SWG waveguides are common features of photonics crystals, the optical equivalent of lattice crystals in solids, of which SWGs are a specific implementation. At the first band-edge of photonic crystals, the band dispersion relation transitions from a quasi-linear band to a completely flat band. Because the group velocity is the first derivative of the dispersion relation, this transition causes a curvature in the band and results in a vanishing group velocity.

The authors are with the Centre d'optique, photonique et Laser (COPL), and the Département de génie électrique et de génie informatique, Université Laval, Québec, QC G1V 0A6, Canada (e-mail: philippe.jean.4@ulaval.ca; antoine.gervais.1@ulaval.ca; sophie.larochelle@gel.ulaval.ca; wei.shi@gel.ulaval.ca).

The phenomenon of structural slow light, that is, low group velocity due to the waveguide structure, is well-known and has been widely studied and used in 2D photonic crystal line-defect waveguides (PhCW) [5]–[7]. In contrast with PhCW, there has been little research and even fewer experimental demonstrations concerned with structural slow light in one-dimensional photonic crystals (1D-PhC), that is, periodic waveguides like SWGs [8]–[10]. Structural slow light can be used in many important applications like on-chip compact delay lines, all-optical switching and signal buffering for optical storage [11]. Furthermore, slow light strongly enhances light-matter interaction in transparent materials and is thus of great interest for non-linear optics [12], lasers [13] and sensing [14], [15].

In this work, we report, for the first time to the authors knowledge, the experimental demonstration of slow light in SWG waveguides. The observation of slow light is achieved by engineering the SWG geometry such that the band-edge is located within the C-band. We present the design and simulation of the waveguides and group index engineering. We experimentally demonstrate high group index (up to 47.74) over a large bandwidth (up to 8.82 nm) with losses lower than 1.5 dB/mm. We show that the waveguides can be designed to operate over a large spectral range simply by varying their period. The experimental results show good agreement with 3D FDTD simulations and the fundamental physics of slow light in 1D-PhC as well as previous work in this field.

The paper is organized as follows. Section II discusses the fundamental physics of slow light in 1D photonic crystals through the use of an analytical model. This analytical model is used to infer the qualitative behaviour of band-edge structural slow light and as an initial design tool. In section III, we present the results of the 3D FDTD simulations and optimized design for slow light operation. In section IV, we present experimental measurements of the group index, the bandwidth and the band-edge shift slope for different SWG variations as well as propagation losses inside and outside the slow light regime for the same waveguides. This section is concluded with a discussion on the origin of slow light loss. Finally, we examine potential improvements on the SWG design and a summary of the results are presented in the last section.

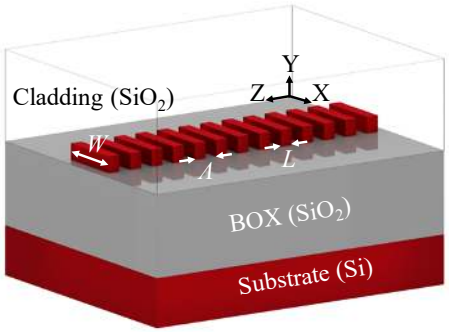

Fig. 1: Schematic of a subwavelength grating waveguide on SOI with width W, silicon block length L and period Λ. The Bloch mode propagates along the Z-axis.

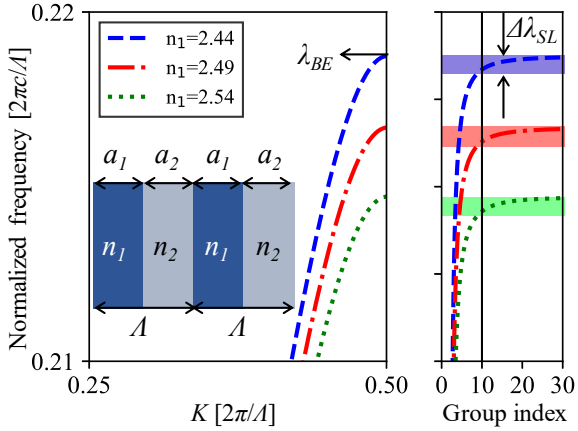

Fig. 2: Analytical dispersion relation at normal incidence (left panel) and group index (right panel) for a 1D-PhC with period $\Lambda = a_1 + a_2 = 330$ nm, duty-cycle of 50% and refractive indices n_1 and $n_2 = 1.44$ (shown as inset).

II. Band-edge waveguide concept: 1D analytical model

In this section, we study the dispersion relation of SWGs by modelling them as 1D-PhC, or periodic stacks of infinite dielectric slabs with index n_1 and n_2, as shown in the inset of figure 2. Because the transverse dimensions are treated as infinite, this model neglects the effect of lateral confinement on waveguide dispersion. The main interest of using this analytical model, in contrast with more accurate methods like 3D FDTD, is the negligible computation time, which is useful to guide initial design choices and infer the physical behaviour of the SWG in the slow light regime. As we will show later, this 1D model faithfully recreates the band curvature near the band-edge. Therefore, the study of 1D-PhC offers great insight into the behaviour of the slow light operation of SWG. The dispersion of a Bloch mode with wavevector K and Bloch effective index n_B follows the relation $K(\omega) = n_B(\omega)\omega/c$ and the dispersion relation of a 1D-PhC at normal incidence is given by [16]:

$$\cos(K\Lambda) = \cos(n_1 a_1 \frac{\omega}{c})\cos(n_2 a_2 \frac{\omega}{c}) - \frac{(n_1^2 + n_2^2)}{(1\sqrt{n_1}\sqrt{n_2})}\sin(n_1 a_1 \frac{\omega}{c})\sin(n_2 a_2 \frac{\omega}{c}) \quad (1)$$

where $n_{1,2}$ and $a_{1,2}$ are the refractive indices and length of each dielectric slab forming the grating, ω is the angular frequency and c is the speed of light in vacuum. The period is then given as $\Lambda = a_1 + a_2$. Knowing the dispersion relation, the group index is easily calculated as $n_g = c\frac{\partial K}{\partial \omega}$. Equation 1 is first solved for a 1D-PhC made of dispersion-less materials $n_1 = [2.44, 2.49, 2.54]$ and $n_2 = 1.44$ with fixed and equal lengths $a_1 = a_2 = 165$ nm ($\Lambda = 330$ nm, $DC = 50\%$). The results are summarized in Fig. 2 with the dispersion relation on the left panel and the corresponding group index on the right panel. The divergent nature of the group index at the onset of the bandgap is evident. The wavelength at which the band becomes flat (infinite group index) is defined as the band-edge position λ_{BE}. The shaded areas in the right panel of Fig. 2 delimit the extent of the slow light regions, which we define as the frequency span over which the group index remains larger than 10. The slow light bandwidth $\Delta\lambda_{SL}$ is then defined as the frequency span between the band-edge and the frequency at which the group index is equal to 10. This definition of band-edge position, slow light region and bandwidth ($n_g \geq 10$) will be used throughout the paper. The zones of lower and higher frequencies outside the slow light region correspond to the SWG and bandgap regimes, respectively.

Because Maxwell's equations tells us that an increase of Λ is equivalent to a decrease of λ and vice-versa, the position of the band-edge can be shifted by varying the period while keeping the same band curvature. This concept will be used and confirmed in the design section and in the experimental results section. We note that the singularity of the group index is a physical concept specific to infinite crystals that cannot be replicated in real, finite devices. Nevertheless, engineering the input and output of the slow light devices can significantly increase the achievable group index in real devices [8], [17].

Next, we solve Eq. 1 for different combinations of parameters to obtain the slow light bandwidth dependence on the 1D-PhC geometry. The results are summarized in Fig. 3. Fig. 3 (a) shows the combined effect of n_1 and duty-cycle on the slow light bandwidth for a 1D-PhC with $n_2 = 1.44$ and $a_2 = 165$ nm while Fig. 3 (b) shows the effect of index contrast ($|n_1 - n_2|$) and averaged index ($\frac{n_1+n_2}{2}$) on the slow light-bandwidth for a 1D-PhC with $a_1 = a_2 = 165$ nm. The bandwidth increases with the index contrast and with the duty-cycle. Therefore, in order to achieve broadband slow light, the gap between the silicon blocks should be left empty (filled with cladding), as is the case for SWGs. These results agree with previous theoretical observations suggesting that fully trenched waveguides offer larger slow light bandwidths

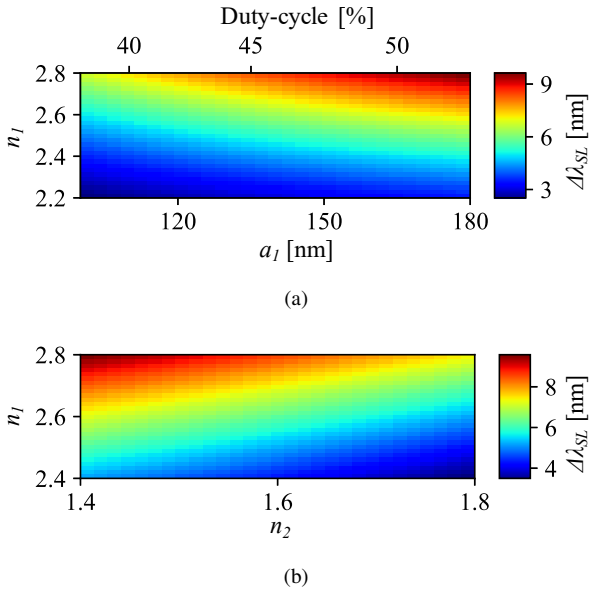

Fig. 3: Slow light bandwidth of a 1D-PhC with(a) $n_2 = 1.44$, $a_2 = 165$ nm and(b) $a_1 = a_2 = 165$ nm

[9]. These last observations indicate that weak gratings are worst for slow light devices. In fact, too weak gratings can even render impossible the experimental observation of slow light due to too small bandwidth [18]. At this point, we note that operation in the dielectric band inherently limits the device bandwidth in contrast with structures propagating higher-order bands with more flexibility for dispersion engineering [7].

III. Design and fabrication

In the previous section, we used an analytical model to approximate the slow light behaviour of band-edge waveguides. More accurate simulations tools are preferable for the design of real devices. Here we use the 3D FDTD algorithm to model the dispersion relation of SWGs operating in the slow light region.

A. 3D FDTD simulation

The simulation is set up around a single unit-cell of length Λ with perfectly matched layer (PML) around the waveguide transverse cross-section and Bloch periodic conditions along the propagation axis. In contrast with the analytical simulation, here the materials dispersion is considered. We designed two variations of the SWGs with widths of 800 nm and 1000 nm and duty-cycles of 50 % and 40 %. In both case, we opted for a wide silicon block to increase the index contrast and achieve a large slow light bandwidth. The reduced duty-cycle (40%) of the second geometry is necessary to prevent multimode operation due to the larger width. Fig. 4 (a) shows the fundamental quasi-TE mode dispersion relation for an SWG with DC=50%, $W = 800$ nm and $\Lambda = 350$ nm. The different operation regimes are identified on Fig. 4, at low frequencies, the dispersion relation becomes linear and the waveguide operates as a metamaterial (SWG regime) with low group index. As the frequency increases, the band goes through the highly dispersive slow light regime and flattens at the band-edge where the forbidden bandgap opens. The blue shaded area delineate the region above the lightline of SiO_2 (n=1.44), above which the geometry supports a continuum of leaky modes.

The top left inset in Fig. 4 depicts a top view of the SWG unit-cell while the four other insets show the normalized electric field intensity of the Bloch mode at different operation points. The Bloch mode profiles in inset are obtained by simulating the same SWG ($DC = 50\%$ and $W = 800$ nm) at 1550 nm with varying periods $\Lambda = 50, 200, 300$ and 350 nm for (i) to (iv), respectively. The Bloch mode profiles correspond to different operation regimes λ/Λ, from the deep-SWG for (i) to the band-edge for (iv). From (i) to (iv), the group indices of the Bloch modes are $n_g = 2.74, 2.92, 3.63$ and 17.37 and the Bloch effective indices are $n_B = 1.82, 1.86, 1.93$ and 2.14. The normalized frequencies and Bloch wavevectors of the modes, from (i) to (iv), are $\omega_n = 0.0323, 0.1290, 0.1935$ and 0.2258 and $K = 0.0589, 0.2394, 0.3733$ and 0.4825. As the band approaches the bandgap and the group index increases, the Bloch mode is reshaped and becomes more concentrated inside the high-index silicon block. The opposite happens in the deep-SWG regime, where the mode sees less of the waveguide periodic variation and the electric field distribution is more spread along the propagation axis.

The phenomenon of Bloch mode reshaping was previously studied in slow light PhCW to explain the non-linear relation observed between group index and extrinsic propagation loss near the band-edge [19], [20]. The localization effect combined with slow light leads to a non-linear increase in light-matter interaction near the band-edge. Furthermore, the mode reshaping leads to a enhancement effect where the higher energy density confinement inside the silicon also reduces the Bloch mode effective area. The combination of these phenomenons indicates a strong potential of band-edge structures and SWGs for increasing the efficiency of non-linear optics processes, which scale with the light-silicon interaction and with the inverse of the effective area. For example, the Bloch mode of inset (i) has an energy density confinement inside the silicon of 54 % compared with 66 % for (iv) while the effective area of the mode goes from a relatively large 0.36 μm^2 at (i) to a very small value of 0.019 μm^2 at the band-edge (iv), an order of magnitude difference.

Fig. 5 shows the group index for the two SWG designs ($DC = 40/50\%$) with a varied period. As the period is increased, the band-edge position is shifted towards longer wavelengths, as expected. The position of the slow light region can thus be shifted over a wide spectral range simply by adjusting the period. The band-edge position varies linearly with the period and, from Fig. 5, this shift is 2.8977 nm/nm and 2.7496 nm/nm for the 40% and 50% SWGs,

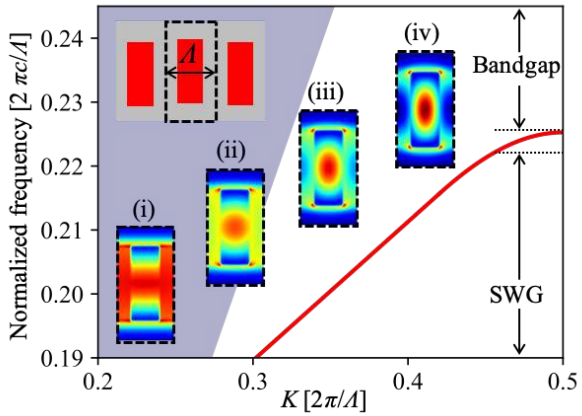

Fig. 4: Dispersion relation calculated using 3D FDTD of the fundamental quasi-TE Bloch mode of an SWG waveguide with DC=50%, $W = 800$ nm and $\Lambda = 350$ nm. The top left inset shows the unit-cell from a top view. Inset (i) to (iv) shows the Bloch mode electric field distribution for various period-to-wavelength ratios.

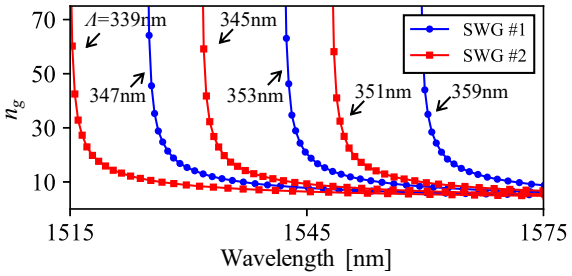

Fig. 5: Group index simulated using FDTD for SWG waveguides with various periods and duty-cycles $DC = 40\%$ (blue circles) and $DC = 50\%$ (red squares).

respectively. This tunability is helpful to design devices operating at a wide range of wavelengths. On the other hand, this implies a relatively weak fabrication tolerance, for example, a systematic misalignment of period of 5 nm would lead to ≈14 nm shift in the position of the slow light region.

B. Device fabrication and test

The devices were fabricated on SOI wafers by electron-beam lithography at Applied NanoTools [21]. The BOX layer was 2.0 microns and the silicon device layer was 220 nm. Light was coupled in and out of the silicon chip using tapered optical fibres (2.5 MFD) and on-chip inverse nanotapers. Mode conversion from the routing strip waveguide to the slow light SWG waveguides was done using physical tapers.The tapers were 500 periods long and thus their exact lengths varied between devices. The period of the taper was linearly changed from 100 nm at the input to the slow light SWG period at the output to prevent crossing into the bandgap. A schematic representation of the strip-to-swg taper is shown in Fig. 6.

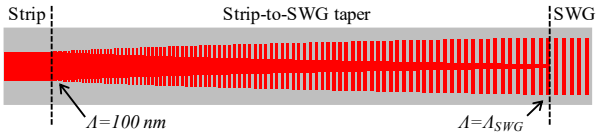

Fig. 6: Top view schematic of the taper used to convert the strip mode (left port) to the slow light SWG mode (right port). The number of taper periods was set to 500 and with a constant input strip waveguide width of 500 nm.

TABLE I: Summary of the fabricated SWG waveguides

	DC [%]	W [nm]	Λ [nm]
SWG #1	40	1000	347 350 353 356 359
SWG #2	50	800	351 354 357 360 363

The spectral and phase responses of the SWGs were measured using an optical vector analyzer (OVA). The group index can be directly calculated from the measured differential group delay and designed device length. Using simulated values of strip waveguide group index to remove the delay caused by the routing sections, the SWG group index is given as:

$$n_{g,swg} = \frac{\tau c - n_{g,strip} L_{strip}}{L_{swg}} \tag{2}$$

where τ is the measured group delay, c is the speed of light in vacuum, L_{swg} and L_{strip} are the length of the SWG and strip waveguides, respectively. For the group index measurements, L_{swg} was set to 2.0 mm. The strip waveguide group index $n_{g,strip}$ is calculated using a finite-difference element solver and ranges from 4.1803 at 1500 nm to 4.1939 at 1600 nm. The group delay and insertion loss measurements from the OVA were noisy due to Fabry-Perot effects caused by the facets and imperfect strip-to-SWG tapers reflections as well as parasitic coupling to slab modes. In order to partially remove the noise and extract the trend of the device response, we applied a Savitsky-Golay smoothing filter to the data.

The parameters of the fabricated SWGs are summarized in table I. For brevity, the SWGs with $DC = 40\%$ and $W = 1000$ nm will be refered to as SWG #1 and SWGs with $DC = 50\%$ and $W = 800$ nm will be refered to as SWG #2 throughout the remainder of the text.

IV. Results and Discussion

In this section, we present experimental results obtained using the methodology described in section III-B.

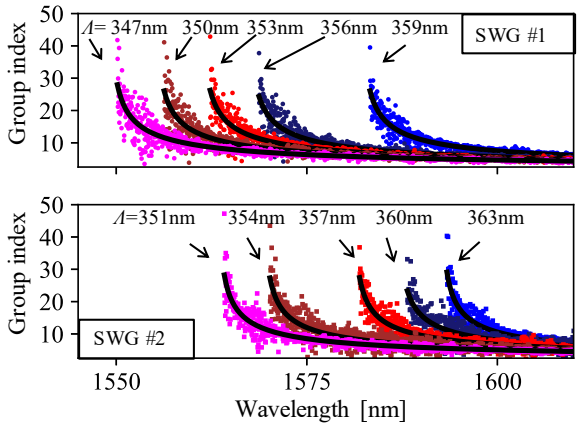

Fig. 7: Measured (markers) group index for the SWG #1 (top) and SWG #2 (bottom). The black full lines shows analytical function fits.

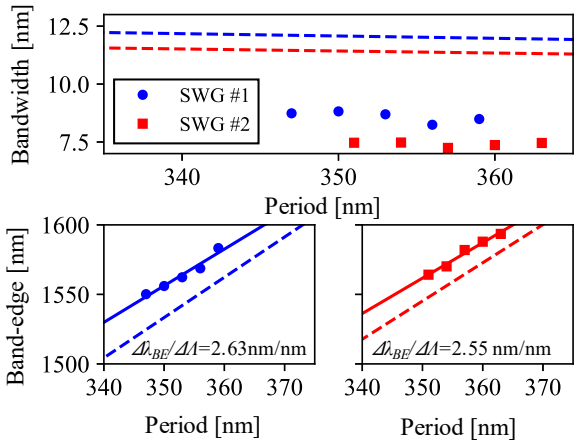

Fig. 8: Top panel: measured (markers) and FDTD simulated (dashed lines) slow light bandwidth for SWG #1 (blue - circles) and SWG #2 (red - squares). Bottom panels: measured (markers) and FDTD simulated (dashed lines) band-edge position for SWG #1 (left - blue circles) and SWG #2 (right - red squares). The solid lines are linear fit to the measured data to extract the shift.

A. Group index

The group index was measured for SWG #1 and #2 with varying periods ranging from 347 nm to 363 nm. The results are summarized in Fig. 7. The maximum measured group index varies between 38.93-43.21 and 34.89-47.74 for SWG #1 and SWG #2, respectively. The full black lines displayed in Fig. 7 are curve fits made using the 1D-PhC analytical dispersion relation of Eq. 1. The maximum measurable group index depends strongly on the input and output tapers of the slow light SWG. Although in simulation a completely flat band, infinite group index and infinite local density of states (LDOS) is easily obtainable due to the infinite extent of the simulated geometry, the finite nature of real devices prevent the group velocity to completely vanish [17]. Multiple methods have been proposed to circumvent the limitation imposed by the finite geometry [8], [9], [17], [22]. As mentioned in the previous section, we opted to implement long physical tapers to convert the routing strip waveguide mode to the slow light SWG Bloch mode. Such physical tapers were previously used with good efficiency to couple light to-and-from the chip [2]. However, the required taper length for an adiabatic transition scales with the group index difference. As such, the measurable group index is strongly dependent on the length of the tapering sections and the length of tapers used here is likely the limiting factor in achieving larger group indices. To a lesser extent, other mechanisms might play a role in limiting the group index, for example, the imaginary part of the material dielectric constant was shown to cause LDOS broadening and to limit the achievable group index [23].

B. Bandwidth and band-edge

We measured the slow light bandwidth $\Delta\lambda_{SL}$ and band-edge wavelength λ_{BE} and compared them with the results from the FDTD simulations. The band-edge is estimated as the wavelength at which the maximum group index is measured. The bandwidth was calculated as the absolute difference between the band-edge position and the wavelength at which the group index is equal to 10, obtained from the analytical fit. The bandwidth (top panel) and band-edge (bottom panel) values extracted from the group index curves are shown in Fig. 8 alongside FDTD simulations for the same devices (dashed lines). The bandwidths obtained from FDTD simulations are ≈12.1 nm and ≈11.5 nm at $\Lambda = 350$nm for SWG #1 and #2, respectively. The slight linear variations are caused by material dispersion; as the period varies, the slow light spectral position shifts, causing a variation of index contrast between the dispersive silicon and silica and a small slope in the bandwidth-period relation. The measured bandwidths (circles and squares) varies from 8.24nm to 8.82nm for SWG #1 and 7.24nm to 7.47nm for the SWG #2. The fluctuations in the trend of $\Delta\lambda_{SL}$ vs Λ can be attributed to dispersion and uncertainty in the analytical fit. The measured bandwidths are systematically narrower in comparison with the FDTD simulation. This discrepancy can be attributed to the finite non-adiabatic tapers mentioned in the previous section. Nevertheless, we observe that the bandwidths for SWG #1 are systematically larger than for SWG #2, which is in agreement with the FDTD data as well as the predictions made using the analytical model (see Fig. 3). This indicates that the higher index contrast provided by the larger silicon block (1000 nm vs 800 nm) results in increased bandwidth even with the reduction effect due to lower duty-cycle (40% vs 50%). Nevertheless, the achievable slow light bandwidth of SWG is limited in contrast with PhCW which profit from more degrees of freedom to control the band curvature and produce larger bandwidth slow light [7], [24].

The measured band-edges are shown in the bottom panel

of Fig. 8. As expected, the band-edge shifts toward the longer wavelength as the period is increased. The measured band-edge shift for SWG #1 and SWG #2 are 2.63 nm/nm and 2.55 nm/nm, respectively. The slope values and trends are comparable to those obtained from FDTD with a systematic shift towards longer wavelength between the simulated and measured band-edges. This systematic deviation can be caused by a difference between the perfect simulated SWG and the fabricated SWG. A slight deviation from the duty-cycle or period can lead to a significant shift in the band-edge position due to its high sensitivity on geometrical parameters, as outlined in section III-A. The deviation could also comes from the difference between the simulated position of band-edge at infinite n_g and the measured band-edge, which is limited to finite group index. The effect of this difference was calculated to be around 1 nm for the measurable group index and thus much smaller than the observed deviation.

C. SWG propagation loss

Next, we present experimental measurements of the transmission in the slow light SWGs. The transmissions of the quasi-TE polarized mode for SWG #1 with $\Lambda = 347$ nm for different lengths (1,2,3 and 4 mm) are presented in Fig. 9 (a) alongside the measured group index (blue circles). We used a standard cutback method to calculate the propagation loss α, which is given as the slope of the linear relation between transmission ($|S_{21}|^2$) and waveguide length (as shown in the inset of Fig. 9 (b)). Although the cutback method provides good agreement with the current experimental data, we note that previous work predicted a non-linear relation for single-mode periodic waveguides [25]. The loss coefficients in dB/mm for SWG #1 with $\Lambda = 347$ nm, 350 nm and 353 nm are shown in Fig. 9 (b) and the inset shows an example of cutback fit. The spectral dependence of the propagation losses are fitted using rational polynomial of degree 3-3. The maximum loss value at the band-edge is close to 12.5 dB/mm for the three periods. The propagation loss coefficient decreases as the wavelength increase to reach a minimum measured value of 1.4 dB/mm. The group index associated with this minimum loss is 4.10, the waveguide then operates well outside of the slow light regime.

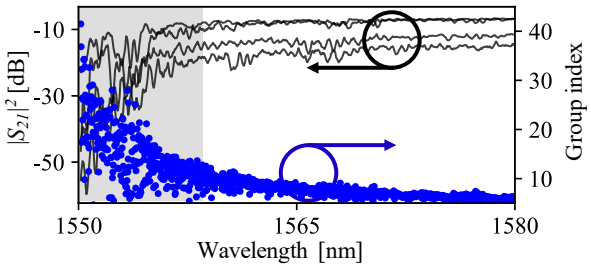

(a)

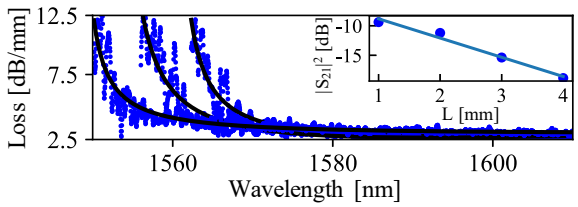

(b)

Fig. 9: (a) Fibre-to-fibre transmission (full black lines) of the slow light device test structure for SWG #1, $\Lambda = 347$ nm and lengths of 1,2,3 and 4 mm (top to bottom) alongside the associated group index (blue circles). (b) Propagation loss in dB/mm for SWG #1 at periods of 347 nm, 350 nm and 353 nm (left to right). The inset of (b) shows a linear fitting to transmission points at 1570 nm for cutback measurements of the propagation loss.

D. Slow light loss

It is well known that structural slow light in photonic crystals comes at the cost of decreased transmission and higher propagation losses due to increased interaction with fabrication defects. The exact mechanism governing optical loss near the band-edge is intricate and has been extensively studied in PhCW [19], [20], [26]–[29]. The theory regarding the loss-group index relationship indicates that two main components are responsible. Out-of-plane scattering causes the light to couple to the leaky continuum of modes supported above the lightline and was shown to scale linearly with n_g. The other mechanism is backscattering, which occurs when a forward mode is scattered and coupled to a backward propagating mode. This second phenomenon is more problematic for slow light as it scales with n_g^2. Additionally, both terms have a strong dependence on the electric field localization, which is itself affected by Bloch mode reshaping as discussed in section III-A. The result of these combined mechanisms is a non-linear relation between the loss and the group index near the band-edge of PhCW which has significant implications for the implementation of slow light. In fact, the reduction of losses in structural slow light devices remains the main challenge of this field. We note that this theory was developed for slow light PhCW and that no similar study has been made for 1D-PhC.

By comparing the propagation losses with the group index data of Fig. 7, we obtain a loss versus group index relationship, as shown in Fig. 10. The blue circles in Fig. 10 shows the measurement points, the black dashed lines shows the relation between the analytical group index fit and the rational polynomial loss fit and the full grey line shows an extended linear fit made on the data outside the slow-light regime ($n_g < 10$). As the group index increases, we observe a clear deviation from the linear regime of loss. This behaviour is in accordance with the non-linear increase of losses in the slow light regime mentioned in the previous paragraph and indicates, to a certain extent, that there is a parallel to make between the theory developed for PhCW and the loss mechanisms at play in 1D-PhC.

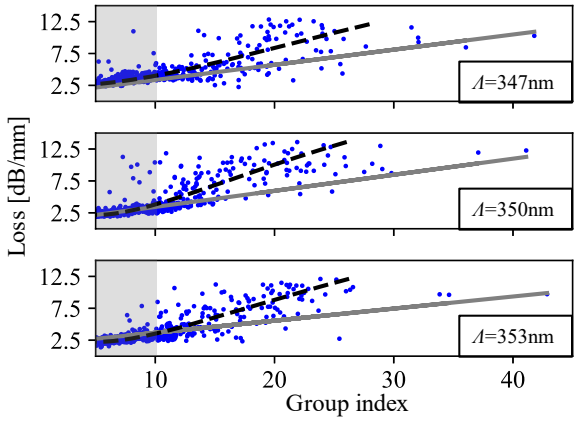

Fig. 10: Propagation loss vs group index relation for SWG #1 at periods of (top) 347 nm, (middle) 350 nm and (bottom) 353 nm. The blue circles show the measurements points, the dashed black lines show the relations between the analytical group index fit and the polynomial loss fit and the solid grey lines show an extended linear fit to the loss data outside the slow-light region with $n_g < 10$ (shaded area).

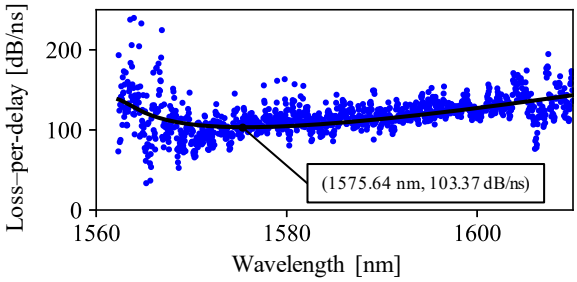

Fig. 11: Loss-per-delay figure of merit for the SWG #1 with $\Lambda = 347$ nm. The blue circles shows the measurement points and the black full line shows the fits relation.

As the interest in slow light lies in reducing footprint and enhancing interaction, the measure of absolute propagation loss is less representative of a device performance. A more sensible and concise representation is the achievable loss per unit time of delay, or loss-per-delay $LD = \alpha c/n_g$, which is used as a common figure of merit in slow light PhCW [7]. The goal of many research efforts in slow light PhCW has been to minimize this value. Various loss reduction methods have been used to enable loss-per-delay in the range of 100 dB/ns with the current state-of-the-art for PhCW reaching values as low as 25 dB/ns [7]. Another approach using coupled PhC cavity recently achieved a record low LD of 15 dB/ns [30]. The loss-per-delay of the SWG #1 with $\Lambda = 347$ nm is shown in Fig. 11 calculated from the raw measurement (blue circles) and using the fitted data (black line). The minimum fitted value is 103.37 dB/ns at 1575.64 nm while the lowest loss-per-delay measured is at 32.15 dB/ns.

The absolute propagation losses of the SWGs are comparable to existing slow light PhCW that can reach 150-300 dB/mm in the slow light regime for group index lower than 100 [18], [28], [31]. Nevertheless, the minimum loss of 1.4 dB/mm, measured well outside of the slow light regime, is almost an order of magnitude larger than the lowest reported loss of 0.21 dB/mm for SWG waveguides operating in the long-wavelength regime [1]. This difference is mainly attributable to the distinct waveguide geometry leading to lower group index ($n_g \approx 1.5$) and to the operation regime as the measurement range did not allow characterization far in the long-wavelength regime. Nevertheless, other factors could have resulted in these higher losses. For example, fabrication imperfections like slanted or collapsed silicon pillars can lead to reduced transmission, this becomes more probable as the number of periods increases in longer waveguides. Also, disorder effects induced losses arising from variations in period alignment along the waveguides could be more prominent in the wider structures [32].

At this point, we emphasize that the Bloch modes are intrinsically lossless, that is, they propagate without diffraction or radiation even when operating near the band-edge. Thus, with perfect fabrication, the SWG waveguides would have no loss albeit the intrinsic material absorption. From a design perspective, the losses could be improved by reducing the silicon block width to reduce disorder effects while cladding the devices in a higher index material would mitigate the effect of roughness. These two modifications would also delocalize the mode away from the silicon blocks and lead to weaker scattering from the etched sidewall roughness. On the other hand, it would also reduce the index contrast, thus narrowing the slow light bandwidth. There is obviously a trade-off to optimize between the bandwidth and the losses. The aforementioned design considerations combined with improved engineering of the structures should lead to significant loss reduction. Furthermore, engineering a strip-to-SWG mode converter or simply increasing the length of the tapers used in this work would greatly improve the performance by allowing the measurements of larger group index.

V. Conclusion

In summary, we experimentally demonstrated slow light in SWG waveguides on SOI for the first time. We measured group index larger than 47 and a slow light bandwidth greater than 8.5 nm. The propagation loss of the waveguides were measured at a relatively low 12.5 dB/mm for the maximum group index with minimum values lower than 1.5 dB/mm well outside the slow-light regime ($n_g < 5$). We finally reported a loss-per-delay figure of merit of 103.37 dB/ns, which is comparable to other 220 nm SOI slow light demonstrations based on PhCW. Various proposed improvements on the design would enable significantly reduced loss-per-delay, making SWGs an excellent solution for on-chip slow light. Furthermore, the simple geometry

of SWGs, their compactness and their operation in the first dielectric band makes them easy to incorporate in existing SOI integrated circuits.

ACKNOWLEDGMENT

We acknowledge the support of the National Sciences and Engineering Research Council through strategic project grant (STPGP 494358-16). This research was partially funded by Sentinel North (project 1.4), a Université Laval CFERF research program, and is also part of the CRC in Advanced Photonic Technologies for Communications.

REFERENCES

[1] P. J. Bock, P. Cheben, J. H. Schmid, J. Lapointe, A. Delâge, S. Janz, G. C. Aers, D.-X. Xu, A. Densmore, and T. J. Hall, "Subwavelength grating periodic structures in silicon-on-insulator: a new type of microphotonic waveguide," *Opt. Express*, vol. 18, no. 19, pp. 20 251–20 262, Sep 2010.

[2] P. Cheben, P. J. Bock, J. H. Schmid, J. Lapointe, S. Janz, D.-X. Xu, A. Densmore, A. Delâge, B. Lamontagne, and T. J. Hall, "Refractive index engineering with subwavelength gratings for efficient microphotonic couplers and planar waveguide multiplexers," *Opt. Lett.*, vol. 35, no. 15, pp. 2526–2528, Aug 2010.

[3] J. G. Wangüemert-Pérez, P. Cheben, A. Ortega-Moñux, C. Alonso-Ramos, D. Pérez-Galacho, R. Halir, I. Molina-Fernández, D.-X. Xu, and J. H. Schmid, "Evanescent field waveguide sensing with subwavelength grating structures in silicon-on-insulator," *Opt. Lett.*, vol. 39, no. 15, pp. 4442–4445, Aug 2014.

[4] P. Cheben, R. Halir, J. H. Schmid, H. A. Atwater, and D. R. Smith, "Subwavelength integrated photonics," *Nature*, vol. 560, no. 7720, pp. 565–572, 2018.

[5] P. Lalanne, S. Coudert, G. Duchateau, S. Dilhaire, and K. Vynck, "Structural slow waves: Parallels between photonic crystals and plasmonic waveguides," *ACS Photonics*, vol. 6, no. 1, pp. 4–17, Jan 2019. [Online]. Available: https://doi.org/10.1021/acsphotonics.8b01337

[6] T. Baba, "Slow light in photonic crystals," *Nature Photonics*, vol. 2, pp. 465 EP –, Aug 2008, review Article.

[7] S. A. Schulz, L. O. Faolain, D. M. Beggs, T. P. White, A. Melloni, and T. F. Krauss, "Dispersion engineered slow light in photonic crystals : a comparison," 2010.

[8] M. L. Povinelli, S. G. Johnson, and J. D. Joannopoulos, "Slow-light, band-edge waveguides for tunable time delays," *Opt. Express*, vol. 13, no. 18, pp. 7145–7159, Sep 2005.

[9] M. Passoni, D. Gerace, L. O'Faolain, and L. C. Andreani, "Optimizing band-edge slow light in silicon-on-insulator waveguide gratings," *Opt. Express*, vol. 26, no. 7, pp. 8470–8478, Apr 2018.

[10] C.-J. Chung, X. Xu, G. Wang, Z. Pan, and R. T. Chen, "On-chip optical true time delay lines featuring one-dimensional fishbone photonic crystal waveguide," *Applied Physics Letters*, vol. 112, no. 7, p. 071104, 2018.

[11] T. F. Krauss, "Why do we need slow light?" *Nature Photonics*, vol. 2, p. 448, aug 2008.

[12] C. Monat, B. Corcoran, D. Pudo, M. Ebnali-Heidari, C. Grillet, M. D. Pelusi, D. J. Moss, B. J. Eggleton, T. P. White, L. O'Faolain, and T. F. Krauss, "Slow light enhanced nonlinear optics in silicon photonic crystal waveguides," *IEEE Journal on Selected Topics in Quantum Electronics*, vol. 16, no. 1, pp. 344–356, 2010.

[13] S. Ek, P. Lunnemann, Y. Chen, E. Semenova, K. Yvind, and J. Mork, "Slow-light-enhanced gain in active photonic crystal waveguides," *Nature Communications*, vol. 5, pp. 1–7, 2014.

[14] C. Kraeh, J. Martinez-Hurtado, A. Popescu, H. Hedler, and J. J. Finley, "Slow light enhanced gas sensing in photonic crystals," *Optical Materials*, vol. 76, pp. 106 – 110, 2018.

[15] A. Gervais, P. Jean, W. Shi, and S. LaRochelle, "Design of slow-light subwavelength grating waveguides for enhanced on-chip methane sensing by absorption spectroscopy," *IEEE Journal of Selected Topics in Quantum Electronics*, vol. 25, no. 3, pp. 1–8, May 2019.

[16] A. Yariv and P. Yeh, *Photonics*. Oxford University Press, 2006.

[17] R. Faggiani, J. Yang, R. Hostein, and P. Lalanne, "Implementing structural slow light on short length scales: the photonic speed bump," *Optica*, vol. 4, no. 4, pp. 393–399, Apr 2017.

[18] M. Notomi, "Manipulating light with strongly modulated photonic crystals," *Reports on Progress in Physics*, vol. 73, no. 9, p. 096501, aug 2010.

[19] S. Hughes, L. Ramunno, J. F. Young, and J. E. Sipe, "Extrinsic optical scattering loss in photonic crystal waveguides: Role of fabrication disorder and photon group velocity," *Phys. Rev. Lett.*, vol. 94, p. 033903, Jan 2005. [Online]. Available: https://link.aps.org/doi/10.1103/PhysRevLett.94.033903

[20] N. Mann, M. Patterson, and S. Hughes, "Role of Bloch mode reshaping and disorder correlation length on scattering losses in slow-light photonic crystal waveguides," *Physical Review B - Condensed Matter and Materials Physics*, vol. 91, no. 24, pp. 1–10, 2015.

[21] L. Chrostowski, H. Shoman, M. Hammood, H. Yun, J. Jhoja, E. Luan, S. Lin, A. Mistry, D. Witt, N. A. F. Jaeger, S. Shekhar, H. Jayatilleka, P. Jean, S. Belanger-de Villers, J. Cauchon, W. Shi, C. Horvath, J. Bachman, K. Setzer, M. Aktary, S. Patrick, R. Bojko, X. Wang, T. Ferreira de Lima, A. Tait, P. Prucnal, D. Hagan, D. Stevanovic, and A. Knights, "Silicon photonic circuit design using rapid prototyping foundry process design kits," *IEEE Journal of Selected Topics in Quantum Electronics*, pp. 1–1, 2019.

[22] P. Pottier, M. Gnan, and R. M. D. L. Rue, "Efficient coupling into slow-light photonic crystal channel guides using photonic crystal tapers," *Opt. Express*, vol. 15, no. 11, pp. 6569–6575, May 2007.

[23] J. Grgić, J. Pedersen, S. Xiao, and N. Mortensen, "Group index limitations in slow-light photonic crystals," *Photonics and Nanostructures - Fundamentals and Applications*, vol. 8, no. 2, pp. 56 – 61, 2010, special Issue PECS 8.

[24] Y. Lai, M. Mohamed, B. Gao, M. Minkov, R. Boyd, V. Savona, R. Houdre, and A. Badolato, "Ultra-wide-band structural slow light," *Scientific Reports*, vol. 8, 12 2018.

[25] A. Baron, S. Mazoyer, W. Smigaj, and P. Lalanne, "Attenuation coefficient of single-mode periodic waveguides," *Phys. Rev. Lett.*, vol. 107, p. 153901, Oct 2011. [Online]. Available: https://link.aps.org/doi/10.1103/PhysRevLett.107.153901

[26] S. Mazoyer, J. P. Hugonin, and P. Lalanne, "Disorder-induced multiple scattering in photonic-crystal waveguides," *Phys. Rev. Lett.*, vol. 103, p. 063903, Aug 2009.

[27] E. Kuramochi, M. Notomi, S. Hughes, A. Shinya, T. Watanabe, and L. Ramunno, "Disorder-induced scattering loss of line-defect waveguides in photonic crystal slabs," *Phys. Rev. B*, vol. 72, p. 161318, Oct 2005.

[28] L. O'Faolain, S. A. Schulz, D. M. Beggs, T. P. White, M. Spasenović, L. Kuipers, F. Morichetti, A. Melloni, S. Mazoyer, J. P. Hugonin, P. Lalanne, and T. F. Krauss, "Loss engineered slow light waveguides," *Opt. Express*, vol. 18, no. 26, pp. 27 627–27 638, Dec 2010.

[29] B. Wang, S. Mazoyer, J. P. Hugonin, and P. Lalanne, "Backscattering in monomode periodic waveguides," *Phys. Rev. B*, vol. 78, p. 245108, Dec 2008.

[30] S. A. Schulz, C. Hu, J. Upham, W. Boyd, L. O. Faolain, S. A. Schulz, C. Hu, J. Upham, and R. W. Boyd, "Controllable low-loss slow light in photonic crystals," vol. 1054806, no. February 2018, 2019.

[31] J. Li, L. OFaolain, S. A. Schulz, and T. F. Krauss, "Low loss propagation in slow light photonic crystal waveguides at group indices up to 60," *Photonics and Nanostructures - Fundamentals and Applications*, vol. 10, no. 4, pp. 589 – 593, 2012, taCoNa-Photonics 2011.

[32] A. Ortega-Moñux, J. Čtyroký, P. Cheben, J. H. Schmid, S. Wang, Íñigo Molina-Fernández, and R. Halir, "Disorder effects in subwavelength grating metamaterial waveguides," *Opt. Express*, vol. 25, no. 11, pp. 12 222–12 236, May 2017.

Philippe Jean Philippe Jean received the B.E. degree in engineering physics in 2015 from the Université Laval, Québec, QC, Canada, where he is currently working towards the Ph.D. degree. His research interests include silicon photonics, lasers and integrated chalcogenides for the MIR.

Antoine Gervais Antoine Gervais received the bachelor's degree in engineering physics in 2017 from the Université Laval, Québec, QC, Canada, where he is currently working toward the M.S degree in electrical engineering at the Centre d'Optique, Photonique et Laser. His research interests include silicon photonic sensing for environmental monitoring and microfluidic.

Sophie LaRochelle Sophie LaRochelle (M'00-SM'13) received the Bachelor's degree in engineering physics from the Université Laval, Quebec, QC, Canada, in 1987, and the Ph.D. degree in optics from the College of Optical Sciences, University of Arizona, Tucson, AZ, USA, in 1992.,From 1992 to 1996, she was a Research Scientist with the Defense Research and Development Canada, Valcartier Research Centre, where she worked on electro-optical systems. Since 1996, she has been a Professor with the Department of Electrical and Computer Engineering, Université Laval, where she holds the Canada Research Chair (Tier 1) in Advanced Photonics Technologies for Communications. Over the years, she has made highly cited contributions in the fields of fiber Bragg gratings, fiber lasers, optical CDMA, and radio over fiber. She has published more than 400 papers in peer-reviewed journals and conferences. Her current research activities focus on optical fibers and integrated devices for optical communication systems including silicon photonic modulators and filters, optical fiber designs for space-division multiplexing and multi-core multi-mode amplifiers.,Dr. LaRochelle is an OSA Fellow.

Wei Shi (S'07-M'12) is an Associate Professor in the Department of Electrical and Computer Engineering, Université Laval, Québec, QC, Canada. He received the Ph.D. degree in electrical and computer engineering from the University of British Columbia, Vancouver, BC, Canada, in 2012, where he was awarded the BCIC Innovation Scholarship for a collaboration entrepreneurship initiative. Before joining Universit Laval in 2013, he was a researcher at McGill University, Montreal, QC, Canada, where he held a Postdoctoral Fellowship from the Natural Sciences and Engineering Research Council of Canada (NSERC). He is currently an Associate Professor with the Department of Electrical and Computer Engineering, Université Laval, Québec, QC, Canada. His current research focuses on integrated photonic devices and systems, involving silicon photonics, nanophotonics, CMOS-photonics co-design, high-speed optical communications, chip-scale lasers, and optical sensors. He is a member of the Center for Optics, Photonics and Lasers (COPL) and holds a Canada Research Chair in Silicon Photonics.